

1 **ON GENERATION OF NODE DISTRIBUTIONS FOR MESHLESS**
2 **PDE DISCRETIZATIONS ***

3 JURE SLAK^{††} AND GREGOR KOSEC[‡]

4 **Abstract.** In this paper we present an algorithm that is able to generate locally regular node
5 layouts with spatially variable nodal density for interiors of arbitrary domains in two, three and higher
6 dimensions. It is demonstrated that the generated node distributions are suitable to use in the RBF-
7 FD method, which is demonstrated by solving thermo-fluid problem in 2D and 3D. Additionally,
8 local minimal spacing guarantees are proven for both uniform and variable nodal densities. The
9 presented algorithm has time complexity $O(N)$ to generate N nodes with constant nodal spacing
10 and $O(N \log N)$ to generate variably spaced nodes. Comparison with existing algorithms is performed
11 in terms of node quality, time complexity, execution time and PDE solution accuracy.

12 **Key words.** Node generation algorithms, Variable density discretizations, Meshless methods
13 for PDEs, RBF-FD

14 **AMS subject classifications.** 65D99, 65N99, 65Y20, 68Q25

15 **1. Introduction.** In recent years, a number of meshless approaches have been
16 developed to numerically solve partial differential equations (PDEs) with the desire
17 to circumvent the problem of polygonization encountered in the classical mesh-based
18 numerical methods. The major advantage of meshless methods is the ability to solve
19 PDEs on a set of scattered nodes, i.e. without a mesh. This advantage was adver-
20 tised even to the point that arbitrary nodes could be used (see [23, p. 14] and [31]),
21 making node generation seemingly trivial. Nevertheless, it soon turned out that such
22 simplification leads to unstable results.

23 Although node placing is considered much easier than mesh generation, certain
24 care still needs to be taken when generating node sets for meshless methods. Many
25 methods require sufficiently regular nodes for adequate precision and stability. Among
26 others, this also holds for the popular Radial Basis Function-generated Finite Differ-
27 ences method (RBF-FD) [12]. Despite the need for quality node distributions, solving
28 PDEs with strong form meshless methods utilizing radial basis functions (RBFs) has
29 become increasingly popular [13], with recent uses in linear elasticity [35], contact
30 problems [36], geosciences [12], fluid mechanics [19], dynamic thermal rating of power
31 lines [21] and even in the financial sector [15].

32 Since one of the key advantages of mesh-free methods is the ability to use highly
33 spatially variable node distributions, which can adapt to irregular geometries and
34 allow for refinement in critical areas, many specialized algorithms for generations of
35 such node layouts have been developed. Most of them can generally be categorized
36 into either mesh-based, iterative, advancing front or sphere-packing algorithms.

37 The most basic way to generate such node sets is to employ existing tools and
38 algorithms for mesh generation, use the generated nodes and simply discard the con-
39 nectivity relations. Such approach was reasoned by Liu [23, p. 14] as: “There are
40 very few dedicated node generators available commercially; thus, we have to use pre-

*Submitted to the editor on December 7th, 2018.

Funding: This work was supported by FWO grant G018916N, the ARRS research core funding no. P2-0095 and Young Researcher program PR-08346.

[†]Faculty of Mathematics and Physics, University of Ljubljana, Jadranska 19, 1000 Ljubljana, Slovenia (jure.slak@ijs.si, <http://e6.ijs.si/~jslack/>).

[‡]“Jožef Stefan” Institute, Department E6, Parallel and Distributed Systems Laboratory, Jamova cesta 39, 1000 Ljubljana, Slovenia (gregor.kosec@ijs.si, <http://e6.ijs.si/~gkosec/>).

processors that have been developed for FEM.”. This is problematic for two reasons: it is computationally wasteful, and some authors have reported that such node layouts yielded unstable operator approximations [32], making them unable to obtain a solution. Besides above shortcomings, such approach is also conceptually flawed, since the purpose of mesh-free methods is to remove meshing from the solution procedure altogether. To this end, other approaches were researched, often inspired by the algorithms for mesh generation.

A common iterative approach is to position nodes by simulating free charged particles, obtaining so-called minimal energy nodes [17]. Other iterative methods include bubble simulation [24], Voronoi relaxation [1] or a combination of both [6]. Iterative methods are computationally expensive and require an initial distribution. Additionally, the user is often required to consider trade-offs between the number of iterations and node quality. Despite their expensive nature, the produced distributions are often of high quality, which makes iterative methods useful for improving node distributions generated by other algorithms [11].

The next category consists of advancing front methods, which usually begin at the boundary and advance towards the domain interior, filling it in the process. Löhner and Oñate [25] present a general advancing front technique that can be used for filling space with arbitrary objects. These methods, especially if generating a mesh, are often restricted to two dimensions [30]. Another example of a two-dimensional advancing front approach is inspired by dropping variable-sized grains into a bucket [11], which yields quality variable density node distributions and is computationally efficient in practice [34].

The last category are the circle or sphere packing methods [22], which generate high quality node distributions, but are often computationally expensive. With inspiration from the graphics community, Poisson disk sampling [7] has become of interest. It can be used to efficiently generate nodes in arbitrary dimensions [5], and has just recently been used as a node generation algorithm [32] providing nodal distributions of sufficient quality for the RBF-FD method.

To the best of our knowledge, algorithms presented in [11, 32] are currently among the best available. However, they have some shortcomings, namely [11] only works in two dimensions and [32] does not support variable nodal spacing. In this paper, we present an algorithm that overcomes these shortcomings. The presented algorithm works in two, three and higher dimensions and supports variable density distributions. It also has minimal spacing guarantees and is provably computationally efficient. The main shortcoming of the presented algorithm is that it requires discretized boundary as an input, which will be addressed in future work. For algorithms that can fill domains with varying density, conformal mappings can be used to generate nodes on curved surfaces by appropriately modifying the node density [11]. The paper by Shankar et al. [32] also includes an algorithm for generation of an appropriate boundary discretization, based on RBF geometric model and super-sampling. This paper does not deal with the task of generating a boundary discretization and focuses on discretizations of domain interiors, assuming that the boundary discretization already exists when required. The extension of the algorithm to curved surfaces will be addressed in future work.

The rest of the paper is organized as follows: in section 2 the requirements for node generation algorithms are discussed, in section 3 recently introduced algorithms for generating nodal distributions, suitable for strong form meshless methods, are presented, in section 4 a new algorithm is presented, in section 5 the algorithms are compared, and some numerical examples are presented in section 6.

91 **2. Node placing algorithm requirements.** In this section we examine a list
 92 of properties that an ideal node-positioning algorithm should possess and discuss the
 93 rationale behind each property. The properties are loosely ordered by decreasing
 94 importance.

- 95 1. *Local regularity.* Nodal distributions produced by the algorithm should be lo-
 96 cally regular throughout the domain, i.e. the distances between nodes should
 97 be approximately equal. This definition of local regularity is somewhat soft
 98 and imprecise. The requirement stems from the fact that local strong form
 99 meshless methods are often sensitive to nodal positions and large discrepan-
 100 cies in distances to the nearest neighbors or other irregularities can cause ill-
 101 conditioned approximations, making the distribution inappropriate for solv-
 102 ing PDEs. Thus, this point should be read in practice as follows: “The
 103 distributions produced by the algorithm should yield quality PDE solutions
 104 when using local strong form methods, if reasonable spacing function h was
 105 given.”.
- 106 2. *Minimal spacing guarantees.* Computational nodes that are positioned too
 107 closely can severely impact the stability of some meshless methods [23]. Thus,
 108 provable minimal spacing guarantees are desirable. For constant spacing h ,
 109 the condition

$$110 \quad (2.1) \quad \|p - q\| \geq h$$

111 is required for any two different points p and q . For variable nodal spacing,
 112 the algorithm should guarantee a local lower bound for internodal spacing.

- 113 3. *Spatially variable densities.* Many node distribution algorithms rely on a con-
 114 stant discretization step h , as do some efficient implementations [5]. Spatially
 115 variable nodal distributions are often required when dealing with irregular
 116 domains or adaptivity [36]. The algorithm should be able to generate distri-
 117 butions with spatially variable nodal spacing, which can be assumed to be
 118 given as a function $h: \mathbb{R}^d \rightarrow (0, \infty)$. The changes in variability should be
 119 gradual and smooth in order to satisfy the requirement of local regularity.
 120 The algorithm should work without any continuity assumptions for reason-
 121 able h (see remarks in subsection 4.3) and should see a constant step h as a
 122 special case of variable step $h(p)$, not the other way around.
- 123 4. *Computational efficiency and scalability.* Time complexity of the algorithm
 124 should ideally be linear in number of generated nodes. Quasilinear time com-
 125 plexity (e.g. $O(N \log N)$) is acceptable, while time complexity that is $\Omega(N^\alpha)$,
 126 for $\alpha > 1$, is undesirable. The algorithm should also be computationally effi-
 127 cient in practice, making it feasible to use as a node generation algorithm in
 128 an adaptive setting.
- 129 5. *Compatibility with boundary discretization.* Assume that a boundary dis-
 130 cretization \mathcal{X}_b of $\partial\Omega$ conforming to the spacing function h , already exists.
 131 More precisely, we are given a set \mathcal{X}_b of points such that for any two neigh-
 132 boring points p and q , the norm $\|p - q\|$ is approximately equal to $h(p)$ or
 133 $h(q)$. The generated discretization of the whole domain Ω should seamlessly
 134 join with the boundary discretization. This helps to prevent problems of-
 135 ten encountered when enforcing boundary conditions (see [32, sec. 3.5] and
 136 references therein).
- 137 6. *Compatibility with irregular domains.* The algorithm should inherently work
 138 with any irregular domain Ω , given its characteristic (i.e. “is element of”)

139 function

$$\begin{aligned}
 &140 \quad \chi_{\Omega}: \mathbb{R}^d \rightarrow \{0, 1\}, \\
 &141 \quad (2.2) \quad \chi_{\Omega}(p) = \begin{cases} 1, & p \in \Omega, \\ 0, & p \notin \Omega. \end{cases} \\
 &142
 \end{aligned}$$

143 Any algorithms that fill axis- or otherwise oriented bounding boxes, or pro-
 144 duce nodes in a certain non-constant space outside Ω are seen as impaired
 145 in this aspect. Desirably, as the volume of Ω decreases, no matter what the
 146 shape of Ω is, so should the number of operations required by the algorithm.

147 7. *Dimension independence.* The algorithm should ideally be formulated for a
 148 general (low) dimension d without any special cases. One-, two- and three-
 149 dimensional versions of the algorithm should also allow a single general im-
 150 plementation.

151 8. *Direction independence.* The produced distributions and running time of the
 152 algorithm should be independent of the orientation of the domain Ω or the
 153 coordinate system used.

154 9. *No free parameters.* The algorithm should aim to minimize the number of free
 155 or tuning parameters and work well for all domains and density functions,
 156 without any user intervention. The aim is to require algorithms to be robust
 157 and work “out of the box”. Any free parameters should be explored and
 158 well understood, default values should be recommended, and varying the
 159 parameters should not drastically change the algorithm’s behavior.

160 10. *Simplicity.* Algorithms with simpler formulations and implementations are
 161 preferred.

162 **3. State of the art algorithms.** To the best of our knowledge, recently pub-
 163 lished algorithms by Fornberg and Flyer [11] and Shankar et al. [32] best satisfy the
 164 requirements described in section 2 and are hence used as a base for further develop-
 165 ment. Both algorithms are first briefly described in the following sections.

166 **3.1. Algorithm by Fornberg and Flyer.** The node positioning algorithm by
 167 Fornberg and Flyer [11] was published in 2015 in a paper titled “Fast generation of 2-D
 168 node distributions for mesh-free PDE discretizations”. The algorithm in its base form
 169 constructs discretizations for two dimensional axis-aligned rectangles and is presented
 170 as Algorithm 3.1. In the following discussion, the first letters of the authors’ surnames
 171 (FF) will be used to refer to the algorithm.

172 Initially, the lower side of the rectangle is filled with nodes, spaced according to
 173 the given spacing function h . The algorithm works as an advancing front algorithm,
 174 starting from $y = y_{\min}$ and advancing towards $y = y_{\max}$. In each iteration the lowest
 175 ($\min(y)$) candidate p from the current list of potential node locations is found, removed
 176 from potential candidates and added to the final list. New candidates are spaced
 177 accordingly away from p and are inserted into the list of potential node locations.
 178 The iteration continues until $y = y_{\max}$ limit is reached.

179 For irregular domains Ω the authors recommend to run the above algorithm for
 180 the bounding box of Ω , denoted $\text{bb}(\Omega)$, and later discard the nodes outside Ω . If
 181 present, the boundary discretization is superimposed onto the discretization generated
 182 by Algorithm 3.1. Additionally, internal nodes whose closest boundary node p is less
 183 than $h(p)/2$ away are discarded as well.

184 A few local “repel algorithm” iterations are recommended in the vicinity of the
 185 boundary to improve the quality. This part will be omitted from consideration, as it

Algorithm 3.1 Node positioning algorithm by Fornberg and Flyer.

Input: Box $[x_{\min}, x_{\max}] \times [y_{\min}, y_{\max}]$, a function $h: [x_{\min}, x_{\max}] \times [y_{\min}, y_{\max}] \rightarrow (0, \infty)$ and $n \in \mathbb{N}$.

Output: An array of points in $[x_{\min}, x_{\max}] \times [y_{\min}, y_{\max}]$ distributed according to h .

```

1: function FF( $x_{\min}, x_{\max}, y_{\min}, y_{\max}, h, n$ )
2:    $pts \leftarrow$  an empty array of points ▷ This is the final array of points.
3:    $candidates \leftarrow$  points spaced according to  $h$  from  $x_{\min}$  to  $x_{\max}$  at  $y$  coordinate  $y_{\min}$  ▷
   This variable represents potential point locations, candidates for actual points that will
   be in the final result.
4:    $(y_{\min}, i_{\min}) \leftarrow$  FINDMINIMUM( $candidates$ ) ▷ Find minimal point with respect to  $y$ 
5:   while  $y_{\min} \leq y_{\max}$  do coordinate and return its value and index.
6:      $p \leftarrow candidates[i_{\min}]$ 
7:     append  $p$  to  $pts$ 
8:     remove points closer than  $h(p)$  from  $candidates$ 
9:     find nearest remaining points in  $candidates$  to the left and to the right of  $p$ 
10:    add  $n$  new points to  $candidates$ , equispaced on the circular sector with center  $p$ ,
    spanning from the nearest left to the nearest right point
11:     $(y_{\min}, i_{\min}) \leftarrow$  FINDMINIMUM( $candidates$ )
12:  end while
13:  return  $pts$ 
14: end function

```

186 is an iterative improvement scheme that can be performed equivalently on any node
 187 distribution generated by any other algorithm [19]. The behavior of FF near the
 188 boundaries is thus excluded from analysis, as it is designed to work with the “repel
 189 algorithm”.

190 **3.1.1. Time complexity analysis.** The complexity of the Algorithm 3.1 is not
 191 given by the authors and is hence derived in this section. Denote the number of
 192 generated nodes with N and the size of array $candidates$ at the start of iteration i
 193 with s_i . Everything up to while loop on line 5 is negligible compared to the main
 194 loop and takes $O(1)$ time for creation of lists and $O(s_0)$ for candidate generation and
 195 minimum extraction. In the main loop, lines 6–7 consume (amortized) constant time
 196 and lines 8–11 take time proportional to the size of $candidates$ array, i.e. $O(s_i)$ time.
 197 Total time complexity is therefore

$$198 \quad (3.1) \quad T_{\text{FFbox}} = O(1) + O(s_0) + \sum_{i=1}^N (O(1) + O(s_i)) = O(N \max_{1 \leq i \leq N} s_i) := O(NS),$$

199 where S is defined as $S = \max_{1 \leq i \leq N} s_i$.

200 Precisely analyzing s_i and S is difficult for general function h . However, for a
 201 fixed square box and constant spacing h it holds that $N = \Theta(\frac{1}{h^2})$ and $s_i = \Theta(n\frac{1}{h}) =$
 202 $\Theta(n\sqrt{N})$. The time complexity in this case is hence $O(nN\sqrt{N})$.

203 For irregular domains Ω additional work is required. If N denotes the final num-
 204 ber of nodes, the algorithm will generate approximately $\frac{|\text{bb}\Omega|}{|\Omega|}N$ nodes in case of
 205 constant h . Superimposing the boundary discretization with N_b nodes and testing all
 206 generated nodes for proximity takes $O(N_b \log N_b + \frac{|\text{bb}\Omega|}{|\Omega|}N \log N_b)$ time, for building
 207 and querying the k -d tree of boundary nodes. These terms are dominated by the node
 208 generation in the interior and the time complexity of the algorithm by Fornberg and

209 Flyer for generating node distributions for irregular domains for constant spacing h is

$$210 \quad (3.2) \quad T_{\text{FF}} = O\left(n \left(\frac{|\text{bb}\Omega|}{|\Omega|} N\right)^{1.5}\right).$$

211 For variable spacing, the overhead of generated nodes due to the irregularity of Ω
 212 and the advancing front size have to be evaluated using integrals, making the time
 213 complexity expression somewhat more complicated and less illustrative.

214 **3.1.2. Implementation notes.** Authors provided a Matlab implementation
 215 of [Algorithm 4.1](#) in the Appendix of their article [11]. This implementation has been
 216 translated to C++ using the Eigen matrix library [16] and the `nanoflann` library
 217 for k -d trees, provided by Blanco and Rai [4]. The translation is mostly faithful to
 218 the original with a few inefficiencies removed. The C++ implementation is approx-
 219 imately 6 times faster than the original Matlab implementation (both tested on the
 220 same computer).

221 **3.2. Algorithm by Shankar, Kirby and Fogelson.** In 2018, Shankar, Kirby
 222 and Fogelson published a node generation algorithm in a paper titled “Robust node
 223 generation for meshfree discretizations on irregular domains and surfaces” [32]. Their
 224 node generation algorithm is designed to work on surfaces and in 3-D, however it
 225 does not support variable nodal spacing. We will focus our attention on the part
 226 that generates discretizations of the domain interior, when boundary discretization
 227 has already been constructed. The main part of the node generation for the interior
 228 is based on Poisson disk sampling of the oriented bounding box $\text{obb}(\Omega)$ of domain
 229 Ω , described in a paper by Bridson [5]. The relevant part of the node generation
 230 algorithm is presented as [Algorithm 3.2](#). In the following discussion the first letters
 231 of the authors’ surnames (SKF) will be used to refer to the algorithm.

232 The algorithm starts by taking points on the boundary and their corresponding
 233 outward unit normals and shifting them towards the domain’s interior by h . An
 234 oriented bounding box (OBB) of the shifted boundary points is then constructed
 235 using Principal Component Analysis (PCA) [18] as described by Dimitrov et al. [10].
 236 The main part of the algorithm, spanning lines 3 to 24, is the Poisson disk sampling
 237 algorithm, which generates the internal discretization of the oriented bounding box
 238 using a background grid G as a spatial search structure. Finally, points outside the
 239 domain, bounded by \mathcal{X} , are discarded. Here, a k -d tree is used to test all candidates
 240 for inclusion by testing against the outward normal of their closest boundary point.
 241 The remaining points along with the original boundary discretization constitute the
 242 final discretization. As an inward-shifted array of points was used to construct the
 243 internal discretization, spacing of at least h is guaranteed.

244 **3.2.1. Time complexity analysis.** Authors themselves provide the time com-
 245 plexity analysis of the algorithm. Translated to our notation, the running time of the
 246 interior fill algorithm is

$$247 \quad (3.3) \quad T_{\text{SKF}} = O\left(n \frac{|\text{obb}(\Omega)|}{|\Omega|} N\right).$$

248 This represents the running time of the Poisson disk sampling. The PCA analysis
 249 and tree construction are linear or log-linear in N_b and are thus dominated by the
 250 Poisson disk sampling.

Algorithm 3.2 Node positioning algorithm by Shankar, Kirby and Fogelson.

Input: Domain Ω and its dimension d .

Input: A nodal spacing step $h > 0$.

Input: A list of boundary points \mathcal{X} of size N_b , moved h towards domain interior.

Output: A list of points in Ω distributed according to spacing function h .

```

1: function SKF( $\Omega, h, \mathcal{X}, n$ )
2:    $obb \leftarrow \text{OBB}(\mathcal{X})$             $\triangleright$  Generate an oriented bounding box of  $\mathcal{X}$  using PCA.
3:    $G \leftarrow d$ -dimensional grid of size  $h/\sqrt{d}$  of  $-1$ .            $\triangleright$  Maps points to their indices.
4:    $p \leftarrow$  uniform random node inside  $obb$ 
5:    $G[\text{INDEX}(p)] \leftarrow 0$             $\triangleright$  INDEX returns  $d$ -d index of  $p$ , and its sequential index is 0.
6:    $S \leftarrow [p]$                         $\triangleright$  Resulting list of accepted samples.
7:    $A \leftarrow \{0\}$                         $\triangleright$  Set of active indices.
8:   while  $A \neq \emptyset$  do
9:      $i \leftarrow \text{RANDOMELEMENT}(A)$             $\triangleright$  Get a uniform random element of  $A$ .
10:     $b \leftarrow \text{false}$                         $\triangleright$  Indicates if any valid points were generated.
11:    for  $j \leftarrow 1$  to  $n$  do
12:       $p \leftarrow$  uniform random point in annulus with center  $S[i]$  and radii  $h$  and  $2h$ 
13:      if not  $\text{OUTSIDE}(p, obb)$  and not  $\text{TOOCLOSE}(p, h, G, S)$  then
14:         $\text{ADD}(A, \text{SIZE}(S))$             $\triangleright$  Add sequential index of  $p$  to active set  $A$ .
15:         $G[\text{INDEX}(p)] \leftarrow \text{SIZE}(S)$             $\triangleright$  Mark grid cell taken by  $p$  as occupied.
16:         $\text{APPEND}(S, p)$             $\triangleright$  Append  $p$  to the list of accepted samples.
17:         $b \leftarrow \text{true}$             $\triangleright$  Flag that an accepted sample was generated.
18:      break for
19:    end if
20:  end for
21:  if  $b = \text{false}$  then            $\triangleright$  Point  $S[i]$  failed to generate any accepted samples.
22:     $\text{REMOVE}(A, i)$             $\triangleright$  Point with index  $i$  is removed from the active set.
23:  end if
24: end while
25:   $T \leftarrow \text{KDTRREENIT}(\mathcal{X})$             $\triangleright$  Initialize spatial search structure on points  $\mathcal{X}$ .
26:   $S \leftarrow \text{FILTER}(T, S)$             $\triangleright$  Discard points outside the region, bounded by  $\mathcal{X}$ .
27:  return  $S$ 
28: end function

```

251 **3.2.2. Implementation notes.** There is a small difference between the algo-
252 rithm as described by Shankar et al. [32] and Bridson [5]. The Bridson version gener-
253 ates up to n candidates for each point and stops as soon as one candidate is accepted.
254 The version in the SKF algorithm generates all n points and adds all accepted candi-
255 dates. Algorithm 3.2 uses the original, Bridson version and to obtain the SKF version,
256 one needs to remove the break statement on line 18. Since the authors of SKF algo-
257 rithm claim to use a faithful implementation of algorithm as presented by Bridson
258 and only list the algorithm for completeness, we decided to use the Bridson version in
259 our tests. All matrix and tensor operations were again implemented using the Eigen
260 matrix library and the k -d tree operations were implemented using `nanoflann`.

261 **4. New node placing algorithm.** From the discussion presented in section 3
262 it is clear that although state of the art placing algorithms provide a solid spatial
263 discretization methodology for strong form meshless methods, there is still room for
264 improvements, especially in the generalization to higher dimensions, flexibility regard-
265 ing variable nodal density, and treatment of irregular domains. Improving upon the
266 work of Fornberg and Flyer [11] and Shankar et al. [32], we propose a new algorithm

267 that overcomes some of limitations of FF and SKF algorithms. We will refer to the
 268 proposed node placing algorithm as PNP in the rest of the paper.

269 The PNP algorithm is, similarly to SKF, based on Poisson disk sampling. Poisson
 270 disk sampling has certain stochastic properties, such as the fact that it produces a
 271 “blue noise distribution” that is an excellent fit for graphical applications like dither-
 272 ing [5, 7]. In context of PDE solution procedure a slightly different distribution is
 273 required that primarily follows appropriate spacing and regularity criteria. There-
 274 fore, the PNP algorithm deviates from the original Poisson disk sampling in order to
 275 effectively produce tightly packed regular distributions needed in solution of PDEs.

276 The PNP algorithm begins either with a given non-empty set of “seed nodes” or
 277 with an empty domain. In the context of PDE discretizations, some nodes on the
 278 boundary are usually already known and can be used as seed nodes, possibly along
 279 with additional nodes in the interior. If algorithm starts with no nodes, it adds a
 280 seed node randomly within the domain. Before the main iteration loop, seed nodes
 281 are put in a queue, waiting to be processed. In each iteration i , a node p_i is dequeued
 282 and *expanded*, by generating a set of candidates C_i , which are positioned on a sphere
 283 with center p_i and radius r_i , where r_i is obtained from the function h , $r_i = h(p_i)$.
 284 Candidates that lie outside of the domain or are too close to already existing nodes are
 285 rejected and remaining candidates are enqueued for expansion. Node p_i is accepted
 286 as a domain node and will not be touched any more. The iteration continues until
 287 the queue is empty. [Figure 1](#) demonstrates a core operation of the algorithm, i.e. the
 288 expansion, with possible selection of new candidates and the rejection process.

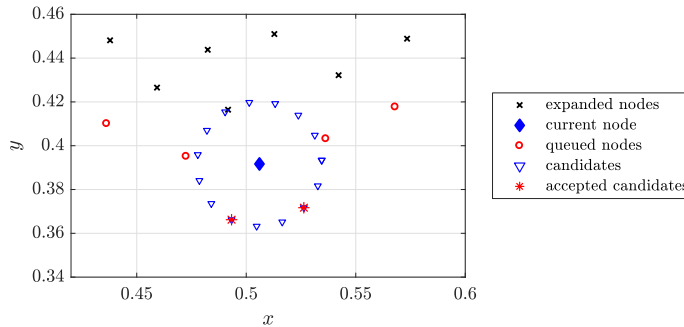


FIG. 1. *Generation and selection of new candidates in the proposed algorithm.*

289 [Figure 2](#) illustrates the execution of the algorithm. The first panel shows an initial
 290 setup on a unit square. For demonstration purposes, the nodes in the initial boundary
 291 discretization along with a single node in the interior were chosen as the seed nodes.
 292 The subsequent panels in [Figure 2](#) illustrate the progression of the algorithm. The
 293 discretization grows from the initial nodes inwards towards the empty interior, until
 294 no more acceptable candidates can be found due to already existing nodes. The
 295 advancing front nature of the algorithm can be seen, however the front itself is not a
 296 straight line as in FF.

297 An efficient implementation with an implicit queue contained in the array of final
 298 points and the k -d tree spatial structure [29] is presented as [Algorithm 4.1](#). In practice,
 299 the comparison on line 10 should be done with some tolerance, due to inexactness of
 300 the floating point arithmetic, i.e. the line should in practice read $\|c_{i,j} - n_{i,j}\| \geq (1 - \varepsilon)r_i$
 301 for e.g. $\varepsilon = 10^{-10}$.

302 The algorithm includes generation of new candidates in line 7 that needs to be

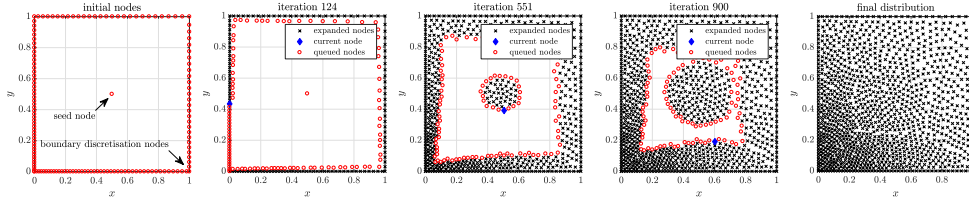


FIG. 2. Run-time progress of the proposed algorithm (left to right). Unit square $[0, 1]^2$ was sampled with nodal spacing function $h(x, y) = 0.015(1 + x + y)$.

Algorithm 4.1 Proposed node positioning algorithm.

Input: Domain Ω and its dimension d .

Input: A nodal spacing function $h: \Omega \subset \mathbb{R}^d \rightarrow (0, \infty)$.

Input: A list of starting points \mathcal{X} , this includes the possible boundary discretization and seed nodes.

Output: A list of points in Ω distributed according to spacing function h .

```

1: function PNP( $\Omega, h, \mathcal{X}$ )
2:    $T \leftarrow$  KDTreeINIT( $\mathcal{X}$ )            $\triangleright$  Initialize spatial search structure on points  $\mathcal{X}$ .
3:    $i \leftarrow 0$                         $\triangleright$  Current node index.
4:   while  $i < |\mathcal{X}|$  do                  $\triangleright$  Until the queue is not empty.
5:      $p_i \leftarrow \mathcal{X}[i]$                 $\triangleright$  Dequeue current point.
6:      $r_i \leftarrow h(p_i)$               $\triangleright$  Compute its nodal spacing.
7:     for each  $c_{i,j}$  in CANDIDATES( $p_i, r_i$ ) do  $\triangleright$  Loop through candidates.
8:       if  $c_{i,j} \in \Omega$  then            $\triangleright$  Discard candidates outside the domain.
9:          $n_{i,j} \leftarrow$  KDTreeCLOSEST( $T, c_{i,j}$ )  $\triangleright$  Find nearest node for proximity test.
10:        if  $\|c_{i,j} - n_{i,j}\| \geq r_i$  then  $\triangleright$  Test that  $c_{i,j}$  is not too close to other nodes.
11:          APPEND( $\mathcal{X}, c_{i,j}$ )              $\triangleright$  Enqueue  $c_{i,j}$  as the last element of  $\mathcal{X}$ .
12:          KDTreeINSERT( $T, c_{i,j}$ )        $\triangleright$  Insert  $c_{i,j}$  into the spatial search structure.
13:        end if
14:      end if
15:    end for
16:     $i \leftarrow i + 1$                     $\triangleright$  Move to the next non-expanded node.
17:  end while
18:  return  $\mathcal{X}$ 
19: end function

```

303 further defined. Three options are proposed and evaluated below:

- 304 1. *Random candidates:* The candidate set C_i in each iteration consists of n
305 random points chosen on a d -dimensional sphere with center p_i and radius r_i ,
306 reminiscing the original Poisson disk sampling.
- 307 2. *Fixed pattern candidates:* The candidate set C_i in each iteration consists
308 of a fixed discretization of a unit ball, translated to p_i and scaled by r_i .
309 The discretization of a unit ball in 2-D is obtained simply by $C_{\text{unit}}(k) =$
310 $\{(\cos \varphi, \sin \varphi); \varphi \in \{0, \varphi_0, 2\varphi_0, \dots, (k-1)\varphi_0\}, \varphi_0 = \frac{2\pi}{k}\}$. In d -dimensions,
311 the discretization of a ball with radius r is obtained using d -dimensional
312 spherical coordinates and recursively discretizing a $d-1$ dimensional ball.
313 Using e.g. $k = 6$ results in 14 candidates in 3-D, and using $k = 12$ results
314 in 48. In 3-D, the parameter k represents the number of points lying on the
315 great circle.
- 316 3. *Randomized pattern candidates:* The candidate set C_i is obtained from the

317 fixed set in point 2, by applying a random rotation to all the points.

318 The three ways of candidate generation were used to produce node distributions
 319 on a unit square, shown in Figure 3. Different types of candidate generation are ab-
 320 breviated as PNP-R, PNP-F and PNP-RF for random, fixed pattern, and randomized
 fixed pattern variants, respectively.

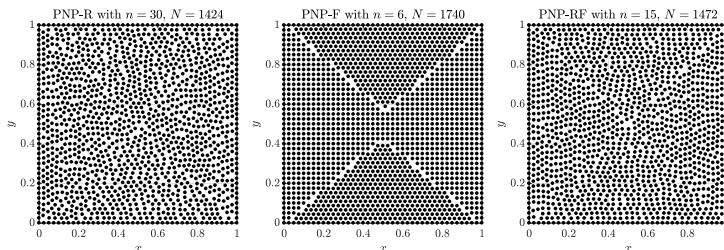


FIG. 3. Comparison of different types of candidate generation when filling the unit square $[0, 1]^2$ with $h = 0.025$.

321

322 The fixed pattern candidate generation algorithm stands out, as the gaps where
 323 the advancing fronts of nodes joined are clearly visible. Due to reproduction of space-
 324 efficient hex-packing it also has the most nodes. Other two algorithms generate visu-
 325 ally similar distributions, but a higher value of n needed to be used for the randomized
 326 version to produce similar results. We decided to use the randomized fixed pattern
 327 for candidate distribution, as it produces results similar to the random version with
 328 lower time complexity.

329 The presented algorithm has a few differences compared to the original Poisson
 330 disk sampling. First and foremost, the algorithm works with variable nodal spacing
 331 and is able to generate distributions with spatially variable densities. Each node is
 332 used only once to generate the new candidates. Third, the candidates are generated
 333 uniformly on the sphere with random offsets, as opposed to being generated at random
 334 on an annulus. This packs the candidates more tightly and reduces the gaps. It also
 335 improves running time, as candidates better cover the unoccupied space at the cost
 336 of removing the stochastic properties of the sampling, which are not relevant to the
 337 PDE solutions. Fourth, the candidates that are outside Ω are immediately discarded,
 338 only continuing the generation of candidates actually inside Ω , once again improv-
 339 ing execution time. More details about impact of above differences are investigated
 340 in section 5 and can be observed in Figure 4 and Figure 11.

341 PNP algorithm exhibits gaps between nodes where the advancing fronts meet
 342 in Figure 3, however the gaps are never large enough that another node could be
 343 placed inside and are even emphasized visually is the marker size is comparable to
 344 nodal spacing (see Figure 4). The exact place where the advancing fronts meet is
 345 dependent on the position of the seed nodes. If the algorithm is run from a seed node
 346 in the domain interior instead of from the boundary nodes, these types of front do
 347 not appear throughout the domain, but gaps form at the boundary instead. With
 348 PDE discretization in mind it is less problematic to have them appear in the domain
 349 interior, and this is how the algorithm is run for the rest of the paper.

350 Additionally, the algorithm can be easily modified to return the indices of the
 351 nodes where the fronts meet. For each node i , we can check if any candidates gener-
 352 ated from it are accepted and added on line 11. If that is not the case, index i can
 353 be added to the list of *terminal nodes*, which is returned after the algorithm finishes.
 354 Regularization can then be performed on those or neighboring nodes, if necessary.

355 **4.1. Time complexity analysis.** Output sensitive time complexity is straight-
 356 forward to analyze. Let us denote the number of given starting points in \mathcal{X} with
 357 $N_b = |\mathcal{X}|$. It is assumed that N_b is significantly less than N , e.g. $N_b = O(N^{\frac{d-1}{d}})$ as is
 358 the case when \mathcal{X} represents the boundary discretization. The initial construction of
 359 the spatial index costs $O(N_b \log N_b)$ and initialization of other variables costs $O(1)$.
 360 The number of iterations of the main loop is equal to the number of generated points,
 361 denoted by N . A total of n candidates are generated in i -th iteration and, in the worst
 362 case, two k -d tree operation on the tree with at most $i + N_b$ nodes are performed,
 363 taking $O(\log(i + N_b))$ time for each candidate. All other operations are (amortized)
 364 constant. Thus the total time complexity of the algorithm is equal to

$$365 \quad (4.1) \quad T_{\text{PNP}} = O(N_b \log N_b) + O(1) + \sum_{i=1}^N [nO(\log(i + N_b)) + O(1)] = O(nN \log N).$$

366 The above analysis shows that the time complexity of the algorithm is dominated
 367 by the spatial search structure used, which adds an undesired factor $\log N$. If h is
 368 assumed to be constant, the algorithm could be sped up by using a uniform-grid based
 369 spatial search structure, similar to one used in [Algorithm 3.2](#). Using such a search
 370 structure requires a rectangular grid, usually with spacing h/\sqrt{d} , such that there is
 371 at most one point per grid cell. When constructed on the rectangle $\text{obb}(\Omega)$, the time
 372 complexity of its allocation and initialization is proportional to the number of cells,
 373 which leads to time complexity

$$374 \quad (4.2) \quad O\left(\frac{|\text{obb} \Omega|}{(h/\sqrt{d})^d}\right) = O\left(\frac{|\text{obb} \Omega|}{|\Omega|} N\right),$$

375 using the fact that for constant h the number of nodes is $N = \Theta(|\Omega|/h^d)$.

376 The subsequent insertions and queries in the grid are all $O(1)$, thus improving
 377 the time complexity of the algorithm for constant h to

$$378 \quad (4.3) \quad T_{\text{PNP-grid}} = O\left(\frac{|\text{obb} \Omega|}{|\Omega|} N + nN\right).$$

379 Furthermore, the factor $\frac{|\text{obb} \Omega|}{|\Omega|}$ can be eliminated by using a hash map of cells instead
 380 of a grid; however, the practical benefit of that approach shows only with very irregular
 381 domains.

382 Using the background grid for a spatial structure is feasible even with moderately
 383 spatially variable h , by allowing more than one point per cell. For even higher vari-
 384 ability, hierarchical grids could be used, but a k -d tree-like search structure is needed
 385 to cover all cases. For a specific use case, k -d tree can be replaced with any spatial
 386 search structure, as desired by the user, obtaining time complexity

$$387 \quad (4.4) \quad T_{\text{PNP-general}} = O(P(N) + Nn(Q(N) + I(N))),$$

388 where P is the precomputation/initialization time used by the data structure on N
 389 nodes, $Q(N)$ is the time spent on a radius query and $I(N)$ is the time spent for new
 390 element insertion.

391 **4.2. Implementation notes.** As in the previous two algorithms, all matrix and
 392 tensor operations were implemented using the Eigen matrix library and the k -d tree
 393 operations were implemented using `nanoflann`.

394 **4.3. Remarks.** Algorithm 3.1 and Algorithm 4.1 do not necessarily terminate,
 395 depending on the nodal spacing function used. The integral

$$396 \quad (4.5) \quad N(h) := \int_{\Omega} \frac{d\Omega}{h(p)^d},$$

397 approximately measures the number of points required and can be infinite even if
 398 function h is smooth and positive on Ω . Simply taking a one dimensional example
 399 $\Omega = (0, 1)$ and $h(x) = \frac{0.1}{x}$ is enough to trick the algorithm into sampling indefinitely.
 400 As a precaution to that and more practically, as a memory limit, the maximal number
 401 of points N_{\max} can be specified by the user and the algorithm can be terminated
 402 prematurely.

403 **5. Satisfaction of the requirements.** This section compares all three node
 404 placing algorithms, namely FF (Algorithm 3.1), SKF (Algorithm 3.2) and PNP (Al-
 405 gorithm 4.1). The results of the comparison presented in this section are summarized
 406 at the end in Table 3. The following subsections roughly follow the requirements
 407 postulated in section 2.

408 **5.1. Local regularity.** The most important feature that an algorithm should
 409 possess is regularity of the distributions. This property is initially tested visually,
 410 by observing plots of nodal distributions, which is feasible only in 2-D. Among other
 411 things, local regularity states also that large discrepancies in distances to nearest
 412 neighbors are not desired. This can be tested in arbitrary dimensions, by observ-
 413 ing distances to nearest neighbors, using various statistics and histogram plots to
 414 determine their properties. Finally, accuracy and stability of solutions of PDEs on
 415 generated node distributions can be compared to fully determine the quality of dis-
 416 tributions generated by the three algorithms.

417 We begin our analyses by comparing the three algorithms on the unit square
 418 $[0, 1] \times [0, 1]$. Node distributions were generated using constant density $h = 0.025$
 419 and the expected number of nodes is $N(h) = 1600$. Node distribution for all three
 420 algorithms are shown in Figure 4. Parameters n for various algorithms were chosen
 421 as recommended in their respective papers ($n = 5$ for FF and $n = 15$ for SKF), with
 422 $n = 15$ also being used for the algorithm presented in this paper.

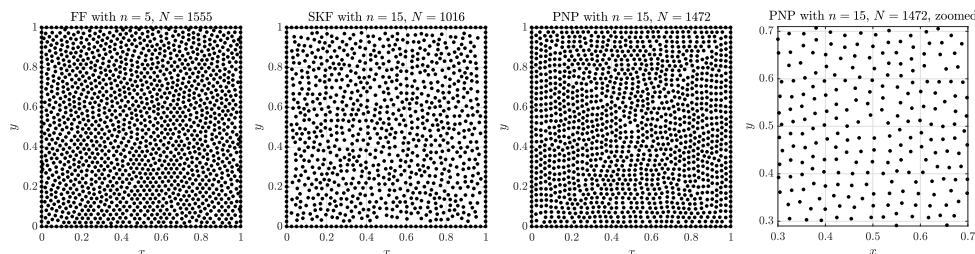


FIG. 4. Node distributions on the unit square $[0, 1]^2$ with $h = 0.025$ generated with different algorithms. Rightmost figure shows the enlarged PNP distribution in the center where the advancing fronts meet.

423 SKF algorithm generated substantially less nodes than the other two. It also has
 424 significant gaps between the boundary and internal nodes as well as visually more
 425 irregular distributions. FF algorithm generates a smooth distribution without any
 426 significant defects in the interior. PNP algorithm exhibits gaps on diagonals, where

427 advancing fronts from the sides have merged, but behaves better near the boundaries.
 428 The part of the distribution where the advancing fronts meet is shown in rightmost
 429 panel in Figure 4 to give a better perspective on the size of the gaps.

430 In terms of the number of nodes, FF gives the best result, since it produced only
 431 45 nodes less than expected, followed by PNP that produces 128 less nodes. The
 432 worst performance is demonstrated by SKF with deficiency of 573 nodes.

433 To analyze local regularity, distances to nearest neighbors are observed in the
 434 interior of the domain. For each node p_i at least $2h$ away from the boundary, its c
 435 closest neighbors (excluding i itself) are found and denoted by $p_{i,j}$ for $j = 1, \dots, c$ with
 436 distances to these neighbors computed as $d_{i,j} = \|p_i - p_{i,j}\|$. Figure 5 shows average
 437 distances of each node to its three closest neighbors, i.e. the plot of $\bar{d}_i = \frac{1}{3} \sum_{j=1}^3 d_{i,j}$
 438 for each considered node p_i . Along with the average distance, the interval $[d_i^{\min}, d_i^{\max}]$
 439 is shown, where

$$440 \quad d_i^{\min} = \min_{j=1,2,3} d_{i,j}, \quad d_i^{\max} = \max_{j=1,2,3} d_{i,j}.$$

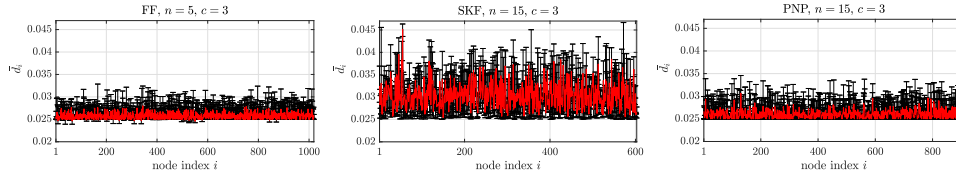


FIG. 5. Average distances to the nearest neighbors for internal nodes. Error bars show minimal and maximal distances to three nearest neighbors.

441 FF and PNP algorithms show similar behavior, with average distance being close
 442 to h with little variability between distances to closest neighbors. FF algorithm has
 443 a few nodes a bit closer than h together, but keeps the internodal distance closer to h
 444 and with less spread than PNP. SKF algorithm performs worse with most of its distances
 445 to c nearest neighbors being on average closer to 0.03 and with a significantly larger
 446 spread. The numerical results representing these quantities are shown in Table 1.
 447 The first two columns of the table demonstrate that the prescribed nodal spacing h is
 448 much better obeyed in PNP and FF algorithms, and the last column shows that the
 449 average spread of the internodal distances in SKF algorithm is more than two times
 450 greater than in FF and PNP.

451 Besides distances to the nearest neighbors, we can also take a look at the empty
 452 space between the generated nodes. This can be done by computing the Voronoi
 453 diagram vertices v_j that lie inside the domain and observing the diameters s_j of the
 454 largest circles centered at v_j not containing any nodes. Formally, s_j are given as

$$455 \quad (5.1) \quad s_j = 2 \min_i \|v_j - p_i\|.$$

456 Note that the largest value of s_j is the diameter of the largest empty circle. The basic
 457 statistics of s_j for the three considered algorithms are presented in Table 1.

458 Additional insight is offered with histograms of distances to three nearest neigh-
 459 bors (Figure 6). As expected, the largest count is in the bin around h . PNP and
 460 SKF algorithms have no distances in bins below h , however the FF algorithm does
 461 put a small number of nodes at a distance less than h (see subsection 5.2). The ir-
 462 regularities visible in the SKF algorithm distribution in Figure 4 are reflected in the
 463 histogram. The histogram has a much heavier tail than PNP and FF histograms,

TABLE 1
Numerical quantities related to internodal distance and hole regularity.

alg.	mean \bar{d}_i	std \bar{d}_i	mean($d_i^{\max} - d_i^{\min}$)	min s_j	mean s_j	max s_j
FF	0.02575	0.00065	0.00208	0.028071	0.03438	0.04352
SKF	0.03042	0.00275	0.02894	0.029737	0.04470	0.07008
PNP	0.02604	0.00086	0.00276	0.028949	0.03568	0.05164

464 with far less nodes exactly at distance h . PNP and FF histograms show more tightly
 465 packed distributions with slimmer tails, however the tail of PNP histogram is a bit
 466 longer and more spread out.

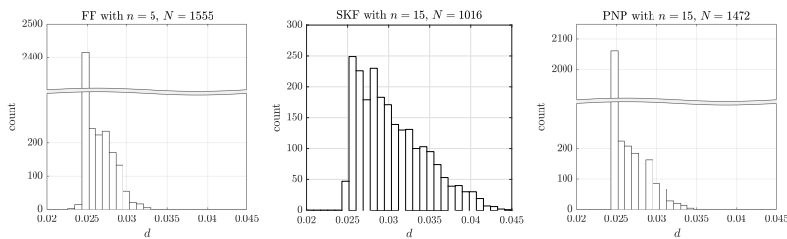


FIG. 6. *Histogram of distances to three nearest neighbors for node distributions on unit square $[0, 1]^2$ with $h = 0.025$.*

467 Next, the PNP and SKF algorithms are compared in three dimensions. The unit
 468 cube $[0, 1] \times [0, 1] \times [0, 1]$ is filled with a constant density $h = 0.05$, starting from
 469 the boundary in the PNP case. The expected number of nodes is $N(h) = 8000$.
 470 Histograms of distances to the closest $c = 6$ nodes for internal nodes are shown
 471 in [Figure 7](#) for PNP and SKF algorithms.

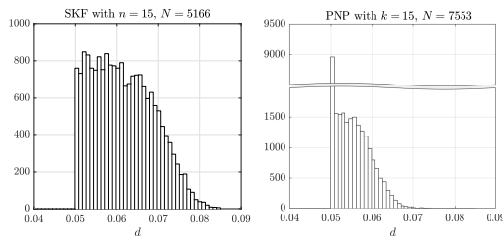


FIG. 7. *Histogram of distances to six nearest neighbors for internal nodes of distributions on unit cube $[0, 1]^3$ with $h = 0.05$.*

472 The histograms behave similarly to their 2-D counterparts. SKF algorithm again
 473 generated significantly less nodes than the PNP algorithm. PNP has a large number
 474 of neighbors at distance h and a lighter tail, while the distances in SKF case are more
 475 spread out.

476 Further visual confirmation of regularity for variable density cases is demonstrated
 477 in [subsection 5.3](#) (see [Figure 9](#), [Figure 10](#) and [Figure 8](#)), and more importantly, by
 478 the solutions of PDEs on generated node sets [\[13, 32, 35\]](#), thus confirming sufficient
 479 local regularity. Additionally, [section 6](#) considers sample solutions to PDE examples
 480 and discusses accuracy, eigenvalue stability and convergence properties. Our experi-
 481 ments have shown that SKF distributions cause stability problems when using small

482 stencils, such as e.g. closest 7 nodes. The likely cause of this instability is higher node
 483 irregularity in SKF node distributions. PNP and FF distributions had no problems
 484 with small stencils.

485 **5.2. Minimal spacing requirements.** Point 2 discusses minimal spacing guar-
 486 antees. Provable minimal spacing guarantees are very desirable, since nodes that are
 487 positioned too closely can effect the stability of strong form methods. FF algorithm
 488 does not strictly respect the spacing h . When running the algorithm with $h = 0.005$
 489 on a unit square $[0, 1]^2$, some pairs of points in the domain interior were closer than
 490 $0.95h$. Although the violations do not appear to be significant and do not affect the
 491 quality in practice, no bound of form $\|p_j - p_i\| \geq \alpha h$, for $\alpha > 0$ and $i \neq j$ is known.

492 SKF algorithm enforces the spacing between nodes to be greater than or equal to
 493 h in the interior and on the boundary, both times leveraging specialized spatial search
 494 structures. The algorithm thus has the usual minimal spacing guarantee for constant
 495 nodal spacing:

496 (5.2)
$$\|p - q\| \geq h$$

497 for $p \neq q$.

498 Similar argument can be made for PNP algorithm: each new candidate is checked
 499 using a k -d tree against all previous ones, proving the minimal spacing guarantee for
 500 constant h . For variable h , the above argument yields the bound

501 (5.3)
$$\|p_i - p_j\| \geq \min_{p \in \Omega} h(p)$$

502 for $i \neq j$. This bound is dependent on a global property of h and can be very
 503 coarse. More precise, local bounds when considering spatially variable distributions
 504 are defined by Mitchell et al. [28]. If an ordered list of points, numbered 1 to N , is
 505 considered, then the minimal spacing guarantee, called the *empty disk property*, is
 506 satisfied if

507 (5.4)
$$\|p_i - p_j\| \geq f(p_i, p_j),$$

508 for $1 \leq i < j \leq N$, where f is a function evaluated at previously accepted node p_i
 509 and new candidate p_j . Four basic variations were proposed, based on which point's
 510 spacing is taken into account when positioning new candidates:

- 511 • *Prior-disks*: $f(p_i, p_j) = h(p_i)$,
- 512 • *Current-disks*: $f(p_i, p_j) = h(p_j)$,
- 513 • *Bigger-disks*: $f(p_i, p_j) = \max\{h(p_i), h(p_j)\}$,
- 514 • *Smaller-disks*: $f(p_i, p_j) = \min\{h(p_i), h(p_j)\}$.

515 The PNP procedure satisfies neither of this variations. The following proposition
 516 establishes a version of the empty disk property (5.4) of PNP.

517 **PREPOSITION 5.1.** *Let the points p_i , $i = 1, \dots, N$, be a list of nodes generated*
 518 *by Algorithm 4.1, where first N_b nodes were given as initial nodes. The minimal*
 519 *spacing inequality*

520 (5.5)
$$\|p_k - p_j\| \geq h(p_{\beta(j)})$$

521 *holds for all $N_b \leq k < j < N$. The function β represents the predecessor function.*

522 *Proof.* Algorithm 4.1 begins with N_b initial nodes. Each candidate is generated
 523 from a unique existing node, thus giving rise to a predecessor-successor relation. Pre-
 524 decessor function $\beta: \{N_b + 1, \dots, N\} \rightarrow \{1, \dots, N\}$ for an accepted candidate p_j that

525 was generated from p_i is defined as $\beta(j) = i$. Note that predecessors for the first N_b
 526 initially given points are not defined.

527 Consider an accepted candidate p_j , generated from a node p_i . The candidate was
 528 generated at a distance $h(p_i)$ from p_i , thus satisfying the equality

$$529 \quad (5.6) \quad \|p_i - p_j\| = h(p_i) = h(p_{\beta(j)}).$$

530 In particular, this means that [Algorithm 4.1](#) satisfies the *prior-disks* property for
 531 predecessor-successor pairs. The distance d to the nearest neighbor of p_j among
 532 already accepted nodes is then found and if $d \geq h(p_i)$, the candidate is accepted.
 533 This means that the following inequality holds for all $k < j$:

$$534 \quad (5.7) \quad \|p_k - p_j\| \geq d \geq h(p_i) = h(p_{\beta(j)}),$$

535 establishing the desired property. \square

536 **5.3. Spatial variability.** An important feature of FF and PNP algorithms is
 537 the ability to generate node sets with variable nodal spacing on irregular domains.
 538 SKF algorithm does not support variable nodal spacing and is excluded from this
 539 analysis. As an example, the image shown in top left corner of [Figure 8](#) is chosen as a
 540 source for the nodal spacing function h . The image is a modified version of an image
 541 showing stress distribution in a plastic spoon under a photoelasticity experiment [2].
 542 It features an irregular domain and rapidly varying dark and light regions, which
 543 presents a more challenging case usually found in PDE discretizations. The conversion
 544 from gray levels to the nodal spacing function is the same as used by Fornberg and
 545 Flyer [11]. Normalization factor $h_0 = 1.5$ was used to adjust the number of nodes for
 546 maximal visibility. The nodal spacing function h is thus constructed from the image
 547 as

$$548 \quad (5.8) \quad h(x, y) = h_0 s \left(\frac{I_{\lfloor wx \rfloor, \lfloor wy \rfloor}}{255} \right), \quad s(g) = 0.002 + 0.006g + 0.012g^8,$$

549 where I_{ij} represents the grey level, ranging from 0 to 255, of the pixel in the i -th
 550 row and the j -th column of the image and w is the width of the image. The node
 551 distributions obtained by filling the spoon shape with aforementioned density using
 552 PNP and FF algorithms are shown in the first row of [Figure 8](#). The bottom row
 553 shows an enlarged portion of the image and the corresponding distributions, so that
 554 individual nodes are visible for easier visual assessment.

555 Both generated node sets conform to the supplied nodal spacing function. The
 556 total number of nodes is similar in both cases, with PNP having fewer nodes than FF.
 557 Enlarged portions show that PNP and FF distributions are locally regular, visually
 558 similar and respect the variable nodal spacing function h .

559 Further examples of 2D and 3D spatially variable distributions are shown in [Fig-](#)
 560 [ure 9](#). The 2D domain is a non-convex polygon with a hole and the 3D domain is a
 561 spherical shell with one of the octants cut out. [Figure 10](#) displays successive enlarge-
 562 ment of a nodal distribution used to solve a contact problem [36], which illustrates
 563 the graded nature of the refinement and its local regularity in the most zoomed panel.

564 **5.4. Computational efficiency and scalability.** Point 4 concerns computa-
 565 tional efficiency in two aspects: theoretical time complexity and execution time.

566 The time complexity of the FF algorithm is proven in [subsection 3.1.1](#) and given
 567 by (3.2)

$$568 \quad (5.9) \quad T_{\text{FF}} = O \left(n \left(\frac{|\text{bb } \Omega|}{|\Omega|} N \right)^{1.5} \right)$$

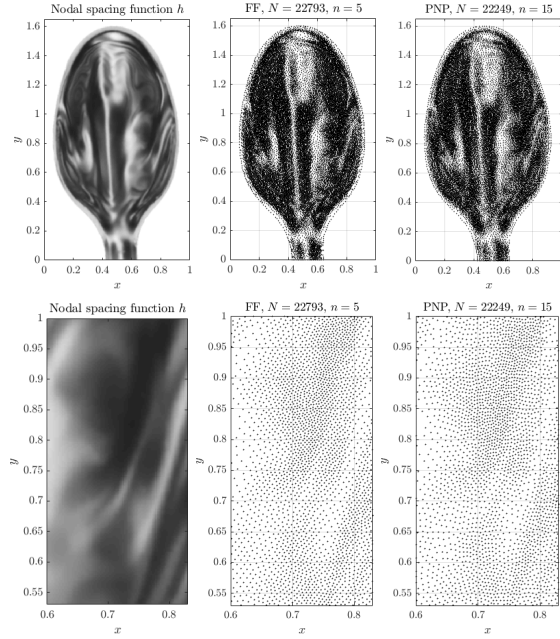


FIG. 8. Illustration of variable density node sampling, with the nodal spacing function h obtained from the image on the left using (5.8). Enlarged variants are present to better assess the node quality.

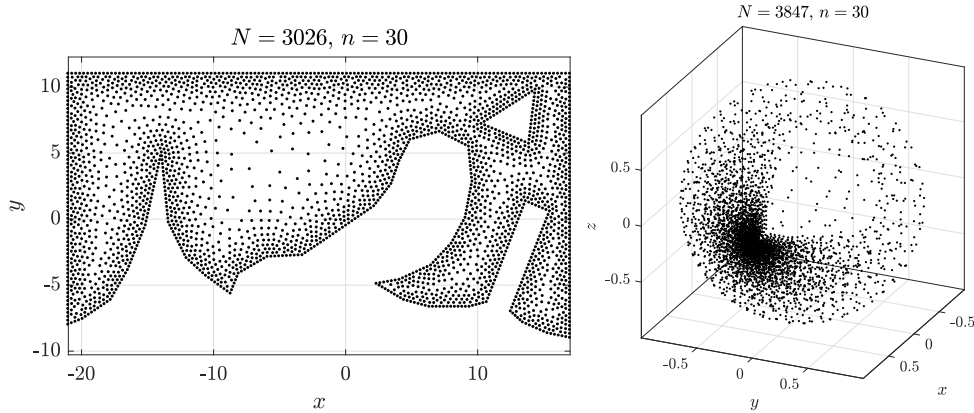


FIG. 9. Example of generated variable density distributions for non-convex domain with non-trivial boundaries.

569 for constant spacing h and is similar for variable spacing. There are no immediate benefits if h is assumed to be constant. The SKF algorithm benefits from the assumption
 570 of constant h and has time complexity given by (3.3) in subsection 3.2.1:
 571

$$572 \quad (5.10) \quad T_{\text{SKF}} = O\left(\frac{|\text{obb}(\Omega)|}{|\Omega|} nN\right).$$

573 PNP algorithm has time complexity

$$574 \quad (5.11) \quad T_{\text{PNP}} = O(nN \log N),$$

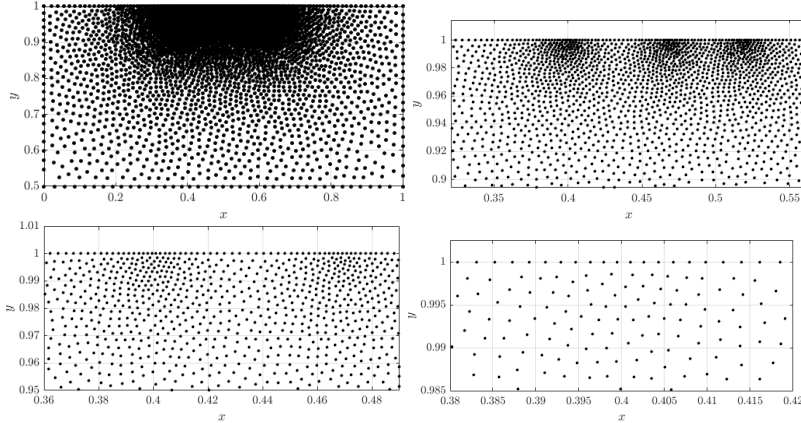


FIG. 10. *Discretisation of a contact region and successive enlargements.*

575 as analyzed in [subsection 4.1](#). If h is assumed constant, the time complexity is further
 576 reduced to $O(\frac{|\text{obb}(\Omega)|}{|\Omega|}N + nN)$ using grid spatial search structure and even to $O(Nn)$
 577 using hashing for irregular domains.

578 PNP algorithm is better for a domain irregularity factor compared to both SKF
 579 and FF algorithms. In case of constant h it shares the same remaining factor Nn
 580 with SKF and for variable densities it is strictly better than FF.

581 Next, we compare the running time and scalability of proposed algorithms. All
 582 time measurements were done on a laptop computer with an Intel(R) Core(TM)
 583 i7-7700HQ CPU @ 2.80GHz processor and 16 GB DDR4 RAM. Code was compiled
 584 using g++ (GCC) 8.1.1 for Linux with `-std=c++11 -O3 -DNDEBUG` flags.

585 Note that we implemented all three algorithms in the same manner with great
 586 emphasis on optimization of the code in order to provide a fair comparison.

587 All algorithms were run on a unit square $[0,1]^2$ with the same parameters as
 588 in [subsection 5.1](#). The nodal spacing function h was varied as $h = \frac{1}{n}$, for such n that
 589 the total number of nodes N reached approximately $N = 10^6$. Each run was executed
 590 10 times and the median time was taken. The results are shown in [Figure 11](#).

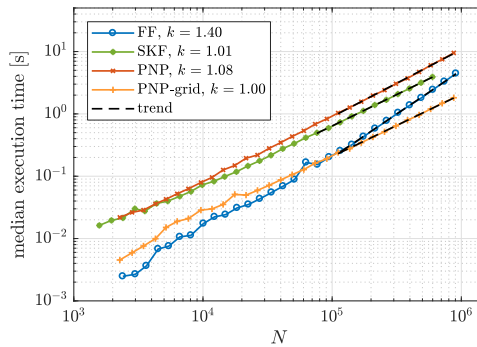


FIG. 11. *Execution times for the considered algorithms when filling $[0,1]^2$ with successively smaller densities. Each data point represents a median of 10 runs. Standard deviation of run times from the median was below 3% in all cases. Value k in the legend indicates slope of the line.*

591 In 2-D the FF algorithm performs better than the others for small N . This is

592 also expected, as the algorithm generates nodes in a much simpler (and deterministic)
 593 way than the other two approaches. SKF algorithm is next in terms of performance,
 594 with its grid-based search structure. PNP algorithm is the slowest, due to the k -d
 595 tree search structure. Nonetheless, 10^6 nodes are generated in 5 to 10 seconds, which
 596 is significantly less than the time that would be spent on solving the PDE on these
 597 nodes.

598 The trends for large N coincide with the theoretical time complexities with SKF
 599 being an $O(N)$ algorithm, PNP being an $O(N \log N)$, and FF being $O(N\sqrt{N})$.

600 PNP was also run using the same grid search structure as SKF, denoted in [Figure 11](#)
 601 by “PNP-grid”. It shows a significant improvement over the use of k -d tree
 602 spatial search structure and agrees with the predicted linear time complexity. This
 603 also shows that PNP algorithm itself is about three times faster than SKF, when
 604 compared using the same search structure and the same number of candidates. PNP
 605 with a grid-based structure also comes close to FF for smaller N and constant h .
 606 Execution time of PNP and SKF algorithms was tested also in 3-D and the results
 607 are equivalent.

608 Additionally, we analyze the execution time of the three algorithms when dealing
 609 with irregular domains. Both FF and SKF algorithms do not have time complexity
 610 proportionate to $|\Omega|$, but rather to the volume of its (oriented) bounding box, which
 611 can be arbitrarily larger. In practice this means that PNP algorithm inherently ben-
 612 efits in execution time by a factor of $\frac{|\text{bb}(\Omega)|}{|\Omega|}$.

613 This is illustrated in [Figure 12](#), which shows the execution time of the considered
 614 algorithms when filling increasingly “emptier” domains

615 (5.12)
$$\Omega(\alpha) = [0, 1]^2 \setminus \left(\frac{1}{2} - \alpha, \frac{1}{2} + \alpha\right)^2.$$

616 Domains $\Omega(\alpha)$ are chosen in such a way that the bounding box is equal to $[0, 1]^2$
 617 for all α and that the limit of the ratio between the bounding box and domain volume
 618 approaches zero as α approaches $1/2$.

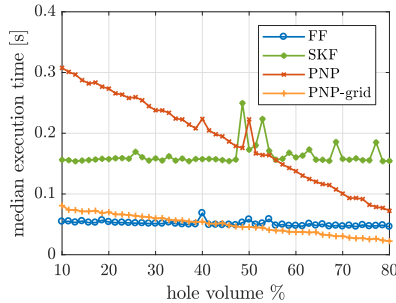


FIG. 12. Execution time when filling domains $\Omega(\alpha)$ which have decreasing area.

619 The difference in the behavior of execution time is substantial and shows that
 620 both versions of PNP really scale with volume of Ω , while the execution time of FF
 621 and SKF remains almost constant, as predicted by time complexity analysis. This
 622 means that around 30 000 nodes can be generated, for less than 8 000 to remain in
 623 the final set.

624 **5.5. Compatibility with boundary discretizations.** The next point dis-
 625 cusses the compatibility between interior and boundary discretizations. All three

626 algorithms treat boundary discretizations separately from discretizing the interior of
 627 Ω . Due to box-fill nature of FF, the generated discretization of the interior is chopped
 628 off at the boundary of Ω when the boundary discretization is superimposed. Nodes
 629 that are closer to the boundary nodes than a given threshold are discarded. If the
 630 threshold is strictly h , gaps between the boundary and the interior discretization can
 631 occur. The authors recommend setting the threshold to $h/2$ and performing a few
 632 iterations of a repel-type algorithm that is executed locally on the nodes near the
 633 boundary to smooth the transition between both discretizations. SKF algorithm pos-
 634 sesses a similar problem, but deals with it differently. It generates internal nodes in a
 635 slightly reduced oriented bounding box, which is computed from boundary nodes that
 636 were shifted by h to the interior. This prevents the generation of internal nodes too
 637 close to the boundary of the box; however, the nodes still need to be tested for inclu-
 638 sion, which is done using the shifted nodes and their normals. This causes gaps near
 639 the boundary, which can be observed in the sample distribution in [Figure 4](#) (second
 640 panel).

641 PNP algorithm bypasses the aforementioned problems altogether, by offering the
 642 option to use the boundary discretization as a starting point of the interior discretiza-
 643 tion and thus allowing for a smooth transition near the boundary. Similar irregu-
 644 larities to those present near the boundary in SKF algorithm are formed when the
 645 advancing fronts from the opposite sides meet, but they appear in the interior of Ω
 646 (see [Figure 4](#), rightmost panel), where they have less impact on the stability of the
 647 solution. Consequently no need to smooth the irregularities with expensive iterative
 648 repel techniques arose.

649 **5.6. Compatibility with irregular domains.** Another requirement deals with
 650 irregular domains. FF algorithm has a disadvantage of being only able to fill axis-
 651 aligned boxes, which results in potentially a lot of unnecessarily generated nodes.
 652 This approach is somewhat improved in the SKF algorithm, where oriented bounding
 653 boxes are used, in general reducing the number of generated nodes compared to FF.
 654 The number of unnecessarily generated nodes could be reduced even further by de-
 655 composing an unfavorably shaped domain into smaller domains, which can be better
 656 bounded by cuboids. The smaller domains can then be filled separately and combined
 657 together, provided that the node generation algorithm behaves well near boundaries.
 658 An appropriate domain decomposition would also enable immediate parallel execution
 659 of the algorithm.

660 Of the three discussed algorithms only PNP never generates any unnecessary
 661 nodes in the exterior of the given domain Ω , never evaluates nodal spacing function h
 662 outside of Ω and has the property that the number total number of generated nodes
 663 and the time complexity scale directly with $|\Omega|$. The impact of unnecessary node
 664 generation outside Ω on the execution time is illustrated in [subsection 5.4](#); however,
 665 the slowdown introduced by bounding boxes is in practice often acceptable.

666 The strength of the PNP algorithm which allows it to generate nodes only inside
 667 Ω can also become its disadvantage. If seed nodes are supplied only in one part of
 668 Ω and the domain has a bottleneck in the middle (such as an hourglass shape) of
 669 girth approximately equal to nodal spacing h in that area, the algorithm might fail
 670 to advance through such bottleneck and would not generate any nodes in the other
 671 part. The FF and SKF algorithms do not suffer from this problem, and it can also be
 672 circumvented in PNP by supplying at least one seed node in each problematic part of
 673 the domain.

674 **5.7. Direction and dimension independence.** Points 7 and 8 deal with di-
 675 rection and dimension independence. FF algorithm is only two-dimensional and di-
 676 rectionally dependent, because the advancing front progresses with respect to the
 677 increasing y coordinate. For inconveniently rotated or badly shaped domains, filling
 678 via increasing last coordinate might perform badly. Choosing a filling direction is
 679 the first step of the algorithm, and it can have significant effect on the running time
 680 and the generated node distribution. The algorithm is also not easily generalizable to
 681 higher dimensions, as it is not immediately obvious how to extend the concept of the
 682 “closest left” point to higher dimensional spaces.

683 The SKF algorithm is better in this aspect. Using PCA it computes oriented
 684 bounded boxes, which provides independence from rotations. The main parts of the
 685 SKF algorithm, i.e. PCA and Poisson Disk Sampling, all work in arbitrary dimensions.
 686 Similarly, all parts of the PNP algorithm are formulated for a general dimension d
 687 and the formulation of the fill procedure is independent of the coordinate system. The
 688 same is true for the implementation: there is a single implementation for all values of d
 689 and the space dimension can truly be a run-time parameter. The coordinates of points
 690 are only accessed in the internals of the k -d tree operations; all other expressions are
 691 coordinate-free.

692 **5.8. Free parameters.** Point 9 states that the developed algorithm should aim
 693 to minimize the number of free or tuning parameters. All three algorithms have
 694 a parameter influencing the number of candidates, which represents a time-quality
 695 trade-off. Authors of FF set $n = 5$ and anything above has similar distributions
 696 with a higher execution time. Authors of SKF analyze the effect of the number of
 697 candidates more precisely and recommend $n = 15$ in 2-D and 3-D, with a higher
 698 number of candidates corresponding to lower errors. For PNP algorithm we similarly
 699 recommend $n = 15$ in 2-D, and $n = 30$ in 3-D with increasing n for higher dimensions.
 700 Anything above $n = 30$ in 2-D gives very similar results and is computationally
 701 wasteful.

702 **6. Solution of PDEs on generated nodes.**

703 **6.1. Poisson’s equation.** The decisive factor of node distribution quality for
 704 strong form methods is its ability to support construction of a good approximations
 705 of differential operators. A basic test of this ability is to solve the Poisson’s equation
 706 on nodes generated by all three algorithms and compare the accuracy of the solutions.

707 A d -dimensional boundary value problem

708
$$\begin{aligned} \nabla^2 u &= f && \text{in } \Omega = [0, 1]^d, \\ u &= 0 && \text{on } \partial\Omega \end{aligned}$$
 709 (6.1)

711 with $u(x_1, \dots, x_d) = \prod_{i=1}^d \sin(\pi x_i)$ and $f(x_1, \dots, x_d) = -d\pi^2 \prod_{i=1}^d \sin(\pi x_i)$ is con-
 712 sidered in $d = 2$ and $d = 3$ dimensions.

713 The solution is obtained using the popular strong form RBF-FD method [13, 26,
 714 35]. Polyharmonic radial basis functions (PHS)

715 (6.2)
$$\varphi(r) = \begin{cases} r^k & k \text{ odd} \\ r^k \log r & k \text{ even} \end{cases}$$

716 with $k = 3$ augmented with monomials up to order 2 are used to construct the
 717 approximations on a stencil of 15 closest nodes in 2-D and 42 closest in 3-D. The final

718 system is solved using BiCGSTAB iterative algorithm with tolerance 10^{-15} and 100
 719 iterations with ILUT preconditioner with fill factor 20 and drop tolerance 10^{-5} .

720 The L^1 error between the correct solution u and obtained solution u_h is evaluated
 721 on an independent uniform grid of points G , three times denser than the densest
 722 discretization used in solution of the problem, and computed as

$$723 \quad (6.3) \quad L^1 = \|u_h - u\|_1 \approx \frac{1}{|G|} \sum_{p \in G} |u(p) - u_h(p)|.$$

724 Node distributions generated by the three considered algorithms are tested using
 725 the same parameters as in [subsection 5.1](#) and [subsection 5.4](#). The nodal spacing
 726 function h varies as $h = \frac{1}{n}$, for such n that the total number of nodes N reached
 727 approximately $N = 10^5$. The results are shown in [Figure 13](#).

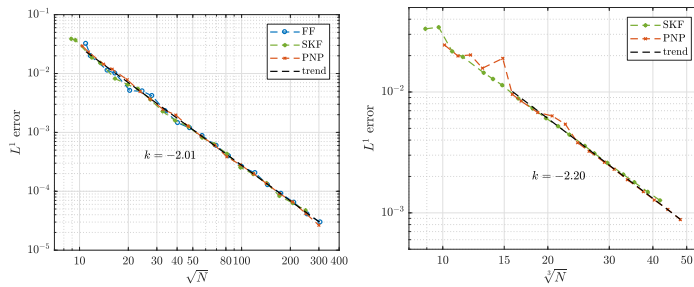


FIG. 13. Accuracy of the numerical solution of (6.1) for considered algorithms when filling $[0, 1]^d$ with successively smaller densities in 2D (left) and 3D (right).

728 In both 2D and 3D case we observe convergence with expected rates for large N .
 729 All node sets give well-behaved solutions with very similar accuracy. Similar results
 730 are obtained in 3D.

731 **6.2. Eigenvalue stability.** An often observed property of numerical discretiza-
 732 tion methods is the spectrum of discretized partial differential operator. For example,
 733 the spectrum of discretized Laplace operator should have only eigenvalues with neg-
 734 ative real part, and a relatively small spread along the imaginary axis [32]. [Figure 14](#)
 735 shows the spectrum of Laplace operator discretized with 2nd order RBF-FD PHS on
 736 PNP nodes shown in [Figure 9](#). There are no eigenvalues with positive real part and
 737 also imaginary spread is relatively small, which additionally confirms the stability of
 738 RBF-FD PHS differentiation on scattered nodes.

739 Additionally, we tested several different setups with different stencil sizes and
 740 approximation orders on nodes distributed with all three positioning algorithms with
 741 minimal differences observed in the spectrum.

742 **6.3. Thermo-fluid problem.** Finally, the PNP algorithm is tested on a more
 743 complex problem. The goal is to demonstrate the capability of meshless solution pro-
 744 cedure on PNP nodes solving a transient non-linear convection dominated problem
 745 in 2D and 3D irregular domain with mixed Dirichlet and Neumann boundary condi-
 746 tions. The natural convection problem governed by coupled Navier-Stokes, mass
 747 continuity and heat transfer equations is chosen for a test case. First, a well-known
 748 de Vahl Davis benchmark test [9] is solved to demonstrate correctness of the solution
 749 procedure, both in 2D and 3D. Once we attain confidence in the solution procedure
 750 we extend the demonstration to irregular domains.

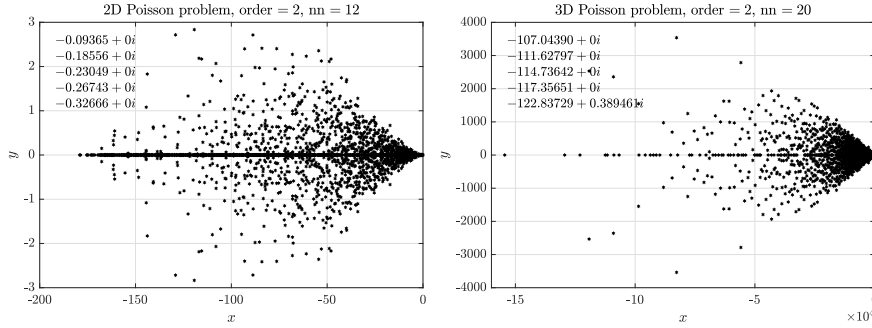


FIG. 14. Spectra of the Laplacian operator discretized with RBF-FD PHS r^3 , augmented with monomials or order 2 on PNP nodes. Note the different scales on the axes of both plots. Variable nn denotes the number of nearest neighbors used to construct the stencil. The 5 eigenvalues with the largest real parts are given in the top left corner of each plot.

751 The natural convection benchmark problem is governed by the following equa-
752 tions:

753 (6.4)
$$\frac{\partial \mathbf{v}}{\partial t} + (\mathbf{v} \cdot \nabla) \mathbf{v} = -\frac{1}{\rho} \nabla p + \frac{\mu}{\rho} \nabla^2 \mathbf{v} + \frac{1}{\rho} \mathbf{b},$$

754 (6.5)
$$\nabla \cdot \mathbf{v} = 0,$$

755 (6.6)
$$\mathbf{b} = \rho(1 - \beta(T - T_{\text{ref}}))\mathbf{g},$$

756 (6.7)
$$\frac{\partial T}{\partial t} + \mathbf{v} \cdot \nabla T = \frac{\lambda}{\rho c_p} \nabla^2 T,$$

757

758 where $\mathbf{v}(u, v, w)$, p , T , μ , λ , c_p , ρ , \mathbf{g} , β , T_{ref} and \mathbf{b} stand for velocity, pressure, tempera-
759 ture, viscosity, thermal conductivity, specific heat, density, gravitational acceleration,
760 coefficient of thermal expansion, reference temperature for Boussinesq approximation,
761 and body force, respectively. The de Vahl Davis test is defined on a unit square do-
762 main Ω , where vertical walls are kept at constant temperatures with ΔT difference
763 between cold and hot side, while horizontal walls are adiabatic. In generalization to
764 3D we assume also front and back walls to be adiabatic [37]. No-slip velocity bound-
765 ary conditions are assumed on all walls. The problem is characterized by Rayleigh
766 (Ra) and Prandtl (Pr) numbers, defined as

767 (6.8)
$$\text{Pr} = \frac{\mu c_p}{\lambda}, \text{Ra} = \frac{g \beta \rho c_p \Delta T h^3}{\lambda \mu},$$

768 with h standing for characteristic length, in our case set to 1. All cases considered in
769 this paper are computed at $\text{Pr} = 0.71$.

770 The problem is solved with implicit time stepping, where each time step begins
771 with a computation of intermediate velocity ($\tilde{\mathbf{v}}_2$)

772 (6.9)
$$\tilde{\mathbf{v}}_2 = \mathbf{v}_1 + \Delta t \left[-(\mathbf{v}_1 \cdot \nabla) \tilde{\mathbf{v}}_2 + \frac{\mu}{\rho} \nabla^2 \tilde{\mathbf{v}}_2 + \frac{1}{\rho} \mathbf{b}(T_1) \right].$$

773 The computed velocity is coupled with mass continuity by an iterative velocity-
774 correction scheme, where it is assumed that the correction depends only on the pres-
775 sure term

776 (6.10)
$$\mathbf{v}_2 = \tilde{\mathbf{v}}_2 - \frac{\Delta t}{\rho} \nabla p.$$

777 Applying divergence on (6.10) yields a pressure Poisson equation

$$778 \quad (6.11) \quad \nabla^2 p = \frac{\rho}{\Delta t} \nabla \cdot \tilde{\mathbf{v}}_2 \text{ in } \Omega, \quad \frac{\partial p}{\partial n} = \frac{\rho}{\Delta t} \tilde{\mathbf{v}}_2 \cdot \mathbf{n} \text{ on } \partial\Omega, \quad \text{subjected to } \int_{\Omega} p = 0,$$

779 which is solved first to get the pressure field. With computed pressure the velocity
 780 is corrected following the (6.10). Steps (6.11) and (6.10) are repeated until the con-
 781 vergence criterion is not met. Once the velocity is satisfactorily divergence free, the
 782 temperature field, coupled with momentum equation through Boussinesq approxima-
 783 tion, is updated as

$$784 \quad (6.12) \quad T_2 = T_1 + \Delta t \left[-\mathbf{v}_2 \cdot \nabla T_2 + \frac{\lambda}{\rho c_p} \nabla^2 T_2 \right].$$

785 All spatial operators are discretized using RBF-FD with r^3 PHS radial basis
 786 functions, augmented with monomials up to order 2, with the closest 25 nodes used
 787 as a stencil. For the time discretization time step $\Delta t = 10^{-3}$ was used for all cases.
 788 Nodal distance $h = 0.01$ is used for simulations in 2D and $h = 0.25$ for simulations
 789 in 3D. Boundaries with Neumann boundary conditions are additionally treated with
 790 ghost nodes [3].

791 In Figure 15 steady state temperature contour and velocity quiver plots for $Ra =$
 792 10^8 case in 2D and $Ra = 10^6$ case in 3D are presented. A more quantitative analysis
 793 is done by comparing characteristic values, i.e. peak positions and values of cross section
 794 velocities, with data available in literature [8, 20, 37, 14]. We analyze six different
 795 cases, namely $Ra = 10^6, 10^7, 10^8$ in 2D, and $Ra = 10^4, 10^5, 10^6$ in 3D. The comparison
 796 in presented in Table 2.

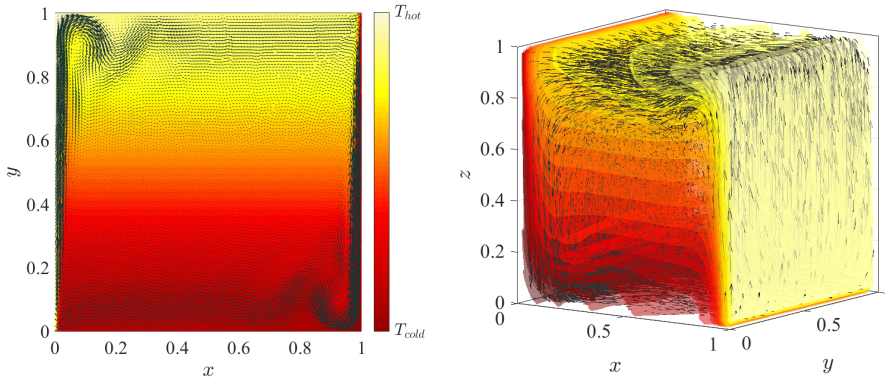


FIG. 15. Temperature contour and velocity quiver plots for $Ra = 10^8$ case in 2D (left) and $Ra = 10^6$ case in 3D (right).

797 Finally, in Figure 16 we demonstrate the solution of transient convection dom-
 798 inated problem in an irregular 2D and 3D domain with mixed Dirichlet-Neumann
 799 boundary conditions on nodes positioned with the proposed algorithm. Note that
 800 this case, a solution of natural convection in an irregular domain, includes several po-
 801 tential complications, such as Neumann boundary conditions on curved boundaries,
 802 concavities, convection dominated transport and non-linearities.

TABLE 2
Comparison of results computed with RBF-FD on FF nodes and reference data.

	Ra	$v_{max}(x, 0.5)$			x			$u_{max}(0.5, y)$			y		
		present	[8]	[20]	present	[8]	[20]	present	[8]	[20]	present	[8]	[20]
2D	10^6	0.2628	0.2604	0.2627	0.037	0.038	0.039	0.0781	0.0765	0.0782	0.847	0.851	0.861
	10^7	0.2633	0.2580	0.2579	0.022	0.023	0.021	0.0588	0.0547	0.0561	0.870	0.888	0.900
	10^8	0.2557	0.2587	0.2487	0.010	0.011	0.009	0.0314	0.0379	0.0331	0.918	0.943	0.930
	Ra	$w_{max}(x, 0.5, 0.5)$			x			$u_{max}(0.5, 0.5, z)$			z		
		present	[37]	[14]	present	[37]	[14]	present	[37]	[14]	present	[37]	[14]
3D	10^4	0.2295	0.2218	0.2252	0.850	0.887	0.883	0.2135	0.1968	0.2013	0.168	0.179	0.183
	10^5	0.2545	0.2442	0.2471	0.940	0.931	0.935	0.1564	0.1426	0.1468	0.144	0.149	0.145
	10^6	0.2564	0.2556	0.2588	0.961	0.965	0.966	0.0841	0.0816	0.0841	0.143	0.140	0.144

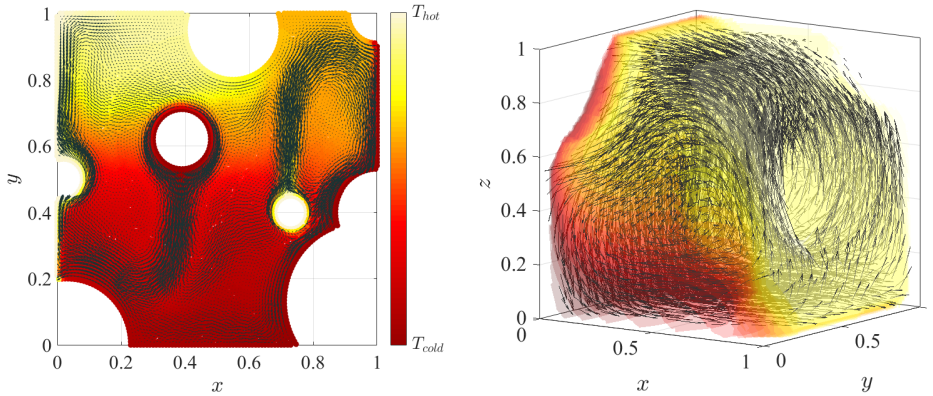


FIG. 16. Temperature contour and velocity quiver plots of solutions in irregular 2D domain (left) and irregular 3D domain (right).

803 **7. Conclusions.** A new algorithm for generating variable density node distri-
 804 butions in interiors of arbitrary dimensions is proposed. The algorithm has many
 805 desirable properties, such as direction independence, support for irregular domains
 806 by only discretizing the area actually contained in the domain interior, good compat-
 807 ibility with boundary discretizations and good scaling behavior. We prove that
 808 the time complexity of the proposed algorithm scales as $O(N)$ for constant spacing
 809 and $O(N \log N)$ for variable spacing. A minimal nodal spacing guarantee for con-
 810 stant and variable nodal spacing functions is also proven. With examples it is shown
 811 that the proposed algorithm produces locally smooth distributions that are suitable
 812 for RBF-FD method for solving partial differential equations. The algorithm is com-
 813 pared against two other state-of-the-art algorithms, and the summary of the findings
 814 is presented in Table 3.

815 The algorithm is also included in the Medusa library [27] for solving PDEs with
 816 strong form meshless methods, but a standalone implementation of the algorithm is
 817 available from the library’s website as well [33].

818 At least three directions are open for future research. The first one deals with
 819 effective adaptive modification of parts of generated distributions with target com-
 820 plexity $O(N_{old} + N_{new})$, where N_{old} and N_{new} stand for the number of removed old
 821 nodes and the number of added new nodes. The second direction is to generalize the

TABLE 3
Comparison of FF, SKF and PNP algorithms.

property / algorithm	FF	SKF	PNP
supports variable density	yes	no	yes
supports 3-D distributions	no	yes	yes
supports irregular domains	yes, using BB	yes, using OBB	yes, natively
compatibility with boundary nodes	n/a	no	yes
dimension independence	no	yes	yes
direction independence	no	yes	yes
randomized	minimal (only starting line)	yes (fully)	yes (controlled)
minimal spacing guarantees	no	yes (constant h)	yes (constant and variable h)
time complexity	$O\left(n\left(\frac{ \text{bb}(\Omega) }{ \Omega }\right)N^{1.5}\right)$	$O\left(n\left(\frac{ \text{obb}(\Omega) }{ \Omega }\right)N\right)$	$O(nN \log N)$ ($O(nN)$ if h constant)
computational time	best for smaller N , 5 s for 10^6 nodes	6 s for 10^6 nodes	10 s for 10^6 nodes, 2 s if h constant
PDE accuracy	satisfactory	satisfactory with larger support sizes	satisfactory
number of free parameters	1 (no. of cand. n)	1 (no. of cand. n)	1 (no. of cand. n)

822 algorithm to (parametric) surfaces, again with desired $O(N)$ time complexity irre-
823 spective of the surface. The third direction is to investigate parallelization opportuni-
824 ties on different parallel architectures ranging from shared memory multi-core central
825 processing units (CPUs) and general purpose graphics processing unit (GPGPUs)
826 to distributed computing. A potential approach, suitable for shared memory, is to
827 independently build the discretization from several seed nodes. The bottleneck in
828 such an approach is the manipulation of global kd-tree search structure, especially
829 on GPGPUS. Alternative simpler search structures, such as spatial grids, could be
830 used instead, as is common practice in computer graphics community. Second option,
831 also suitable for distributed computing, is via domain decomposition, where main
832 problems arise in load balancing and appropriate partitioning of the complex higher
833 dimensional domains.

834 **Acknowledgments.** The authors would like to acknowledge the financial sup-
835 port of the Research Foundation Flanders (FWO), The Luxembourg National Re-
836 search Fund (FNR) and Slovenian Research Agency (ARRS) in the framework of the
837 FWO Lead Agency project: G018916N Multi-analysis of fretting fatigue using phys-
838 ical and virtual experiments, the ARRS research core funding No. P2-0095 and the
839 Young Researcher program PR-08346.

840

REFERENCES

- 841 [1] M. BALZER, T. SCHLÖMER, AND O. DEUSSEN, *Capacity-constrained point distributions: a vari-*
842 *ant of Lloyd's method*, ACM Transactions on Graphics, 28 (2009), [https://doi.org/10.](https://doi.org/10.1145/1531326.1531392)
843 [1145/1531326.1531392](https://doi.org/10.1145/1531326.1531392).
844 [2] S. BAUER, *Image Number K7245-1*. United States Department of Agriculture, [https://www.](https://www.ars.usda.gov/oc/images/photos/k7245-1/)
845 [ars.usda.gov/oc/images/photos/k7245-1/](https://www.ars.usda.gov/oc/images/photos/k7245-1/).
846 [3] V. BAYONA, N. FLYER, B. FORNBERG, AND G. A. BARNETT, *On the role of polynomials in*
847 *RBF-FD approximations: II. Numerical solution of elliptic PDEs*, J. Comput. Phys., 332
848 (2017), pp. 257–273, <https://doi.org/10.1016/j.jcp.2016.12.008>.

- 849 [4] J. L. BLANCO AND P. K. RAI, *nanoflann: a C++ header-only fork of FLANN, a library for*
850 *nearest neighbor (NN) with KD-trees*, 2014, <https://github.com/jlblancoc/nanoflann>.
- 851 [5] R. BRIDSON, *Fast Poisson disk sampling in arbitrary dimensions*, in SIGGRAPH sketches,
852 2007, p. 22, <https://doi.org/10.1145/1278780.1278807>.
- 853 [6] Y. CHOI AND S. KIM, *Node generation scheme for meshfree method by Voronoi diagram and*
854 *weighted bubble packing*, in Fifth us national congress on computational mechanics, Boul-
855 der, CO, 1999.
- 856 [7] R. L. COOK, *Stochastic sampling in computer graphics*, ACM Trans. Graphics, 5 (1986), pp. 51–
857 72, <https://doi.org/10.1145/7529.8927>.
- 858 [8] H. COUTURIER AND S. SADAT, *Performance and accuracy of a meshless method for laminar*
859 *natural convection*, Numerical Heat Transfer: Part B: Fundamentals, 37 (2000), pp. 455–
860 467, <https://doi.org/10.1080/10407790050051146>.
- 861 [9] G. DE VAHL DAVIS, *Natural convection of air in a square cavity: A bench mark numerical*
862 *solution*, Int. J. Numer. Methods Fluids, 3 (1983), pp. 249–264, <https://doi.org/10.1002/fld.1650030305>.
- 863 [10] D. DIMITROV, C. KNAUER, K. KRIEGEL, AND G. ROTE, *On the bounding boxes obtained by*
864 *principal component analysis*, in 22nd European Workshop on Computational Geometry,
865 2006, pp. 193–196.
- 866 [11] B. FORNBERG AND N. FLYER, *Fast generation of 2-D node distributions for mesh-free PDE*
867 *discretizations*, Computers & Mathematics with Applications, 69 (2015), p. 531–544, <https://doi.org/10.1016/j.camwa.2015.01.009>.
- 868 [12] B. FORNBERG AND N. FLYER, *A primer on radial basis functions with applications to the*
869 *geosciences*, SIAM, 2015, <https://doi.org/10.1137/1.9781611974041>.
- 870 [13] B. FORNBERG AND N. FLYER, *Solving PDEs with radial basis functions*, Acta Numerica, 24
871 (2015), p. 215–258, <https://doi.org/10.1017/S0962492914000130>.
- 872 [14] T. FUSEGI, J. M. HYUN, K. KUWAHARA, AND B. FAROUK, *A numerical study of three-*
873 *dimensional natural convection in a differentially heated cubical enclosure*, Int. J. Heat
874 Mass Transfer, 34 (1991), pp. 1543–1557, [https://doi.org/10.1016/0017-9310\(91\)90295-p](https://doi.org/10.1016/0017-9310(91)90295-p).
- 875 [15] A. GOLBABAI AND E. MOHEBIANFAR, *A new method for evaluating options based on multi-*
876 *quadric RBF-FD method*, Appl. Math. Comput., 308 (2017), pp. 130–141, <https://doi.org/10.1016/j.amc.2017.03.019>.
- 877 [16] G. GUENNEBAUD, B. JACOB, ET AL., *Eigen v3*, 2010, <http://eigen.tuxfamily.org>.
- 878 [17] D. P. HARDIN AND E. B. SAFF, *Discretizing manifolds via minimum energy points*, Notices of
879 the AMS, 51 (2004), pp. 1186–1194.
- 880 [18] I. JOLLIFFE, *Principal component analysis*, Springer Series in Statistics, Springer, 2nd ed., 2011,
881 https://doi.org/10.1007/978-3-642-04898-2_455.
- 882 [19] G. KOSEC, *A local numerical solution of a fluid-flow problem on an irregular domain*, Adv.
883 Eng. Software, 120 (2018), pp. 36–44, <https://doi.org/10.1016/j.advengsoft.2016.05.010>.
- 884 [20] G. KOSEC AND B. ŠARLER, *Solution of thermo-fluid problems by collocation with local pressure*
885 *correction*, International Journal of Numerical Methods for Heat & Fluid Flow, 18 (2008),
886 pp. 868–882, <https://doi.org/10.1108/09615530810898999>.
- 887 [21] G. KOSEC AND J. SLAK, *RBF-FD based dynamic thermal rating of overhead power lines*, in
888 Advances in Fluid Mechanics XII, vol. 120 of WIT transactions on engineering sciences,
889 Wessex institute, WIT press, 2018, pp. 255–262, <https://doi.org/10.2495/afm180261>.
- 890 [22] X.-Y. LI, S.-H. TENG, AND A. UNGOR, *Point placement for meshless methods using sphere*
891 *packing and advancing front methods*, in ICCES’00, Los Angeles, CA, Citeseer, 2000.
- 892 [23] G.-R. LIU, *Mesh free methods: moving beyond the finite element method*, CRC press, 2002,
893 <https://doi.org/10.1201/9781420040586>.
- 894 [24] Y. LIU, Y. NIE, W. ZHANG, AND L. WANG, *Node placement method by bubble simulation and*
895 *its application*, Computer Modeling in Engineering and Sciences(CMES), 55 (2010), p. 89,
896 <https://doi.org/10.3970/cmcs.2010.055.089>.
- 897 [25] R. LÖHNER AND E. OÑATE, *A general advancing front technique for filling space with arbitrary*
898 *objects*, Int. J. Numer. Methods Eng., 61 (2004), pp. 1977–1991, <https://doi.org/10.1002/nme.1068>.
- 899 [26] B. MAVRIČ AND B. ŠARLER, *Local radial basis function collocation method for linear thermo-*
900 *elasticity in two dimensions*, Int. J. Numer. Methods Heat Fluid Flow, 25 (2015), pp. 1488–
901 1510, <https://doi.org/10.1108/hff-11-2014-0359>.
- 902 [27] *Medusa library*, <http://e6.ijs.si/medusa/>.
- 903 [28] S. A. MITCHELL, A. RAND, M. S. EBEIDA, AND C. BAJAJ, *Variable radii Poisson-disk sam-*
904 *pling, extended version*, in Proceedings of the 24th canadian conference on computational
905 geometry, vol. 5, 2012.
- 906 [29] A. W. MOORE, *An introductory tutorial on kd-trees*, 1991, <https://doi.org/10.1.1.28.6468>.

- 911 [30] P.-O. PERSSON AND G. STRANG, *A simple mesh generator in MATLAB*, SIAM Rev., 46 (2004),
912 pp. 329–345, <https://doi.org/10.1137/s0036144503429121>.
- 913 [31] K. REUTHER, B. SARLER, AND M. RETTENMAYR, *Solving diffusion problems on an unstructured,*
914 *amorphous grid by a meshless method*, Int. J. Therm. Sci., 51 (2012), pp. 16–22, <https://doi.org/10.1016/j.ijthermalsci.2011.08.017>.
915
- 916 [32] V. SHANKAR, R. M. KIRBY, AND A. L. FOGELSON, *Robust node generation for meshfree dis-*
917 *cretizations on irregular domains and surfaces*, SIAM J. Sci. Comput., 40 (2018), pp. 2584–
918 2608, <https://doi.org/10.1137/17m114090x>.
- 919 [33] J. SLAK AND G. KOSEC, *Standalone implementation of the proposed node placing algorithm.*
920 <http://e6.ijs.si/medusa/static/PNP.zip>.
- 921 [34] J. SLAK AND G. KOSEC, *Fast generation of variable density node distributions for mesh-free*
922 *methods*, in WIT Transactions on Engineering Sciences, vol. 122, 2018, [https://doi.org/10.](https://doi.org/10.2495/be410151)
923 [2495/be410151](https://doi.org/10.2495/be410151).
- 924 [35] J. SLAK AND G. KOSEC, *Refined meshless local strong form solution of Cauchy–Navier equation*
925 *on an irregular domain*, Eng. Anal. Boundary Elem., (2018), [https://doi.org/10.1016/j.](https://doi.org/10.1016/j.enganabound.2018.01.001)
926 [enganabound.2018.01.001](https://doi.org/10.1016/j.enganabound.2018.01.001).
- 927 [36] J. SLAK AND G. KOSEC, *Adaptive radial basis function-generated finite differences method for*
928 *contact problems*, Int. J. Numer. Methods Eng., (2019), <https://doi.org/10.1002/nme.6067>.
- 929 [37] P. WANG, Y. ZHANG, AND Z. GUO, *Numerical study of three-dimensional natural convection*
930 *in a cubical cavity at high Rayleigh numbers*, Int. J. Heat Mass Transfer, 113 (2017),
931 pp. 217–228, <https://doi.org/10.1016/j.ijheatmasstransfer.2017.05.057>.